Shape programmable chitosan films as soft microrobots toward the development of chemo-mechanical sensors

Kailas Mahipal Malappuram, Aritra Chatterjee, Srishti Chakraborty, Souvik Debnath, Kaushik Chatterjee*, Amit Nain*

K. M. Malappuram, S. Chakraborty, S. Debnath, K. Chatterjee, A. Nain
Department of Material Engineering, Indian Institute of Science, Bangalore (560012), Karnataka, India

A. Chatterjee
Department of Mechanical Engineering, Birla Institute of Technology and Science-Pilani, Hyderabad Campus, Medchal (500078), Telangana, India

K. Chatterjee
Department of Bioengineering, Indian Institute of Science, Bangalore (560012), Karnataka, India

A. Nain
Department of Applied Mechanics & Biomedical Engineering, Indian Institute of Technology, Madras (600036), Tamil Nadu, India

*Corresponding author (s)
Email addresses: kchatterjee@iisc.ac.in (K. C.) & amitnain@iisc.ac.in; amitnain0183@gmail.com (A. N.)

Abstract

Shape-morphing materials showed tremendous potential in soft robotics; however, such mechanodynamic behavior has never been applied to develop a sensing platform. Achieving true reversibility in these materials is the goal that so far remains a significant challenge. Our work presents a monocomponent chitosan film fabricated using a solvent-casting method. Beyond exhibiting instantly reversible shape-morphing, a rare feat in itself, the film demonstrates a remarkable bidirectional capability in response to alkaline solution. The film responds rapidly to a specific stimulus – water – undergoing dramatic shape changes with a high bending angle in minimal time, owing to the spontaneous diffusive gradient. This responsiveness is further enhanced by the ability to program the shape simply by tailoring the aspect ratio of the film. Further, precise control over locomotion was achieved by arresting the deformed structure in a transient state via a solvent exchange (water-ethanol-water) process. We utilized this solvent-responsive behavior to demonstrate a proof of concept for detecting alcohol by creating a 'strip-on-a-drop' based chemo-mechanical sensor. Programmed deformation combined with MATLAB-based digital image processing algorithms provided bending angles that consistently quantify alcohol content in a droplet. We believe our film offers a versatile platform for developing on-demand shape control with exciting possibilities.

Graphical abstract

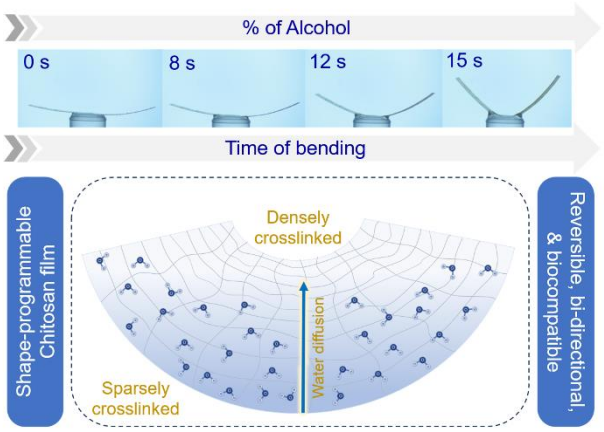

1 Introduction

The natural world abounds with organisms that exhibit remarkable shape-shifting abilities in response to external stimuli[1]. From the pinecone's hygroscopic response that facilitates seed dispersal to the inchworm's programmable dynamic body contortions for locomotion, these transformations offer a captivating glimpse into the ingenuity of biological design[2–6]. Underlying these shape changes are intricate mechanisms involving the formation of gradients and anisotropic swelling within the organism[7,8]. Driven by a deep fascination with these biological marvels, researchers have increasingly focused on deciphering the principles governing such drastic morphological alterations. This growing body of knowledge serves as a springboard for developing biomimetic materials – synthetic materials that emulate the properties and functionalities observed in nature[9]. These "smart" materials, including electroactive polymers[10] and responsive hydrogels[11], can undergo controlled shape changes. This biomimetic approach holds immense potential to transform various fields. Artificial muscles[12], inspired by natural tissues, could power innovative robots and prosthetics. Reconfigurable scaffolds[13–15], constructed from these materials, could revolutionize tissue engineering by providing dynamic cell growth and regeneration environments. The future of soft robotics[16–18] also appears brighter, with programmable materials enabling the creation of robots with superior dexterity and adaptability. This exploration of bioinspired, shape-shifting materials represents a significant leap forward, offering exciting possibilities for a wide range of applications. Recent advancements in material science, coupled with our expanding understanding of biological morphing, have opened doors to the development of bioinspired actuators[19,20]. These actuators are artificial components that can convert energy into controlled motion. By incorporating concepts gleaned from nature, such as responsive materials and hierarchical structures, researchers are now engineering actuators that exhibit complex shape transformations [21,22]. These biomimetic actuators can potentially revolutionize various fields, ranging from targeted drug delivery to soft robotics[19,23]. Over the past decade, researchers have dedicated significant efforts to creating this phenomenon using man-made materials[24,25].

Traditionally, this morphing behavior has been achieved by incorporating various components within the hydrogel structure, each exhibiting distinct responses regarding dimensional changes upon exposure to specific stimuli. For instance, bilayer hydrogels have been utilized, where an "active" layer with a pronounced response in dimensional change is combined with a "passive" layer to generate deformations based on the resulting mismatch strain[26,27]. While previous studies, such as the works of Alsberg et al., have demonstrated reversible shape transformations in hydrogels[28], our group recently achieved both reversibility and bidirectionality in a four-dimensional (4D)-printed material[29]. This functionality was attributed to the unique gradient and multi-component structure created through the three-dimensional (3D) printing process. However, the prolonged response time remains a significant

hurdle, requiring approximately 45 minutes for a solvent-induced transformation. Additionally, the limited bending angle of around 250° achieved within this timeframe restricts its applicability in fields like surgery or cargo delivery, where faster and more pronounced shape changes are often necessary[30,31]. While this multi-component strategy offers advantages, it also has inherent limitations. The interfaces between these components can be unstable; fabrication processes can be time-consuming, and the overall design might not be readily adaptable for biomedical applications[32]. Developing monocomponent hydrogel films capable of precisely controlled shape transformations remains a critical research focus. While some researchers have addressed this challenge by creating monocomponent hydrogels with internal structural gradients, often fabricated using 3D printing[33–35], these approaches can be complex and expensive. Toward this, Hue et al.[36] demonstrated monocomponent shape-morphing behavior in a natural polysaccharide chitosan hydrogel prepared via solvent casting and crosslinked with glutaraldehyde. This method offers a simpler and more cost-effective approach, eliminating the need for 3D printers and intricate crosslinking techniques. However, using glutaraldehyde for crosslinking presents a significant limitation for biomedical applications due to its cytotoxicity, hindering cell viability studies. Additionally, the study by Hue et al. does not explore the reversibility or bi-directionality of the shape-morphing behavior.

To achieve the desired properties in an efficient and economical manner, we present a novel monocomponent chitosan film exhibiting a unique combination of properties highly desirable for soft robotic and chemo-mechanical sensing applications. The film demonstrates rapid, reversible shape-morphing behavior responsive to water, facilitated by a spontaneous diffusive gradient. This responsiveness is further enhanced by programmable shape control through aspect ratio manipulation. Additionally, we showcase the ability to arrest the deformed structure for precise locomotion control via a solvent exchange process. The potential of this film as a sensing platform is established through a proof-of-concept alcohol detection system, leveraging a "strip-on-a-drop" approach coupled with digital image processing. This versatile platform offers exciting possibilities for developing on-demand shape control with potential applications in soft robotics, microfluidics, and lab-on-a-chip devices. Future investigations will explore the integration of this film with various actuating mechanisms and explore its suitability for more complex sensing applications.

2 Results and Discussion

Mono-component chitosan (CHT) film was fabricated using solvent-casting[36]. A homogenous dispersion of CHT in acidic conditions (acetic acid 5% vol./vol.) was poured into a Teflon petri dish and slowly evaporated at ambient conditions (**Fig. S1**). This gradual evaporation process facilitates the removal of water content from the solution, ultimately forming a dry plastic-like CHT film. However, it is essential to note that during this natural drying, the partial and slow escaping water molecules induced asymmetric stress distribution within the film structure[37]. Further, dried CHT film could quickly change their shapes in response to moisture (< 30s) (**Fig. 1A**). The observed shape deformation upon partial water contact is attributed to diffusive hydration, a process where water molecules passively move from areas of high concentration to areas of low concentration due to osmotic pressure gradients[38]. The initial flat film undergoes a gradual folding (primary deformation, denoted as 1°) and unfolding (secondary deformation, denoted as 2°) sequence along a predictable and repeatable path. The observed symmetrical folding pattern, initiated from both sides of the film, renders a strong dependence on the AR[37]. Interestingly, the AR significantly influences the resulting deformation patterns (**Fig. 1A**). Films with the lowest AR, i.e., 1, rolled from two ends to form a tubular structure (**movie S1**). In contrast, films with an AR of 6, characterized by a greater length, demonstrated a rolling tendency accompanied by rotation along the longer axis, ultimately forming a helical structure (**movie S2**). A distinct spiral rolling pattern was observed for films with an AR of 30 resembling narrow strips

(**movie S3**). Finally, films with the highest AR (AR = 60) exhibited a complex dual-spiral rolling behavior (**movie S4**).

The temporal evolution of the film's folding and unfolding behavior was quantitatively evaluated by recording the bending angle (θ) at designated time points (**Fig. 1B**). The bending angle is the angular measure formed by the arc created by the film's deformation, envisioned as part of a complete circle[36]. A flat (unbent) and fully rolled (circle) corresponds to a θ of 0°and 360°, respectively. This methodology quantifies the film's shape transformation throughout the dynamic folding and unfolding process (**Fig. 1C**). Stimuli-responsive materials exhibit aspect ratio-dependent shape morphing. This variation arises because changes in the relative dimensions (length, width, thickness) influence the distribution of internal stresses and actuation forces during the response[39–41] . Prior research has documented shape-morphing films capable of folding behavior. However, the extent of bending observed in the present CHT film surpasses that reported for any other material. For films with an AR of 1, the θ reaches 760°, yielding a concentric tube architecture. For AR 6, θ was 1080°, effectively completing three full circular rotations. Notably, the spiral (AR=30; θ~1000°) and dual-spiral (AR=60; θ~2700°) structures displayed the formation of intricate concentric circles. Following the programmed folding into designated three-dimensional structures, it will stay in the folded state for ~5 seconds and, subsequently, undergo reversible shape-morphism, returning to its original state. This rapid unfolding highlights the material's responsive nature and underscores its potential for applications requiring dynamic shape reconfiguration. Furthermore, these films achieve a significantly higher bending angle than previously reported materials, demonstrating their exceptional shape-morphing capabilities.

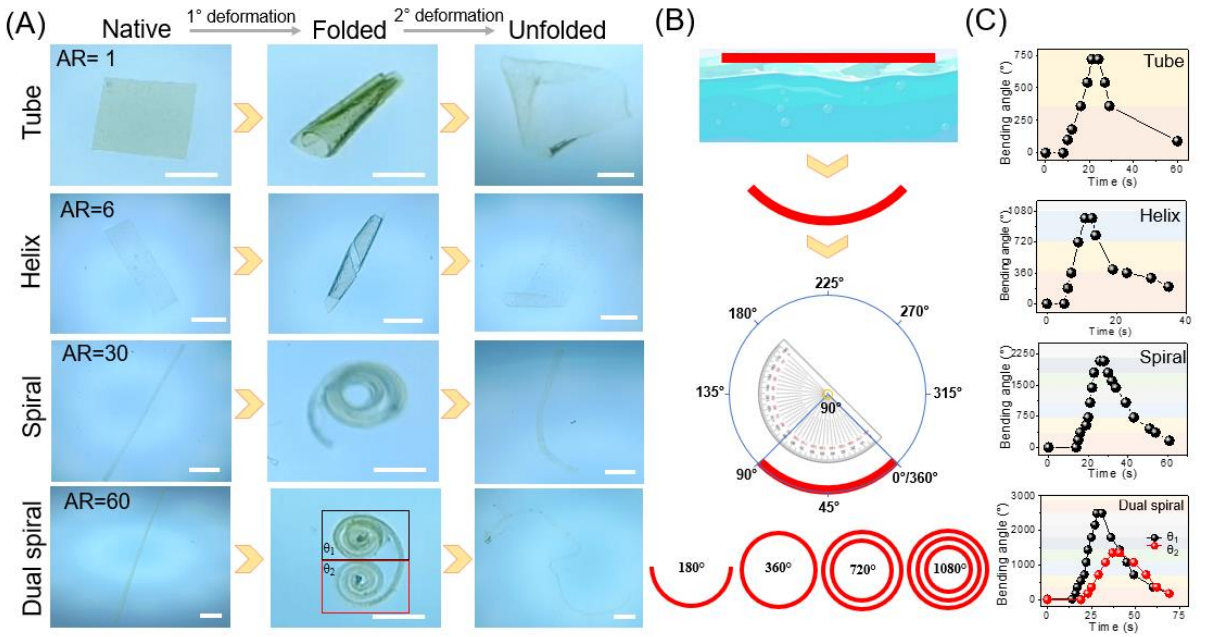

Figure 1
(A) The images show the native-folded-unfolded states of the various CHT films on contact with the water surface. (B) Schematic of calculating the bending angle. (C) Bending angle of the corresponding shape deformations. Scale bar = 5 mm.

Further, the influence of film thickness on folding-unfolding behavior was investigated (**Fig. S2**). To elucidate the impact of film thickness on spiral rolling behavior, CHT films with varying thicknesses (0.01 mm, 0.04 mm, and 0.07 mm) were evaluated under identical testing conditions with an AR of 30 (**Fig. S2**). Films with a thickness of 0.01 mm exhibited improper rolling, hindering the determination of bending angles (**Movie S5**). This phenomenon can be attributed to the rapid diffusive transport of

water molecules associated with the low film thickness. While films with a thickness of 0.04 mm demonstrated proper rolling, their performance was inferior to that observed for the 0.07 mm films (**Movie S6 and S3**). This suggests the existence of an optimal water diffusion rate for efficient spiral rolling. Films with a thickness of 0.07 mm likely establish a more favorable water concentration gradient within their structure, facilitating superior folding and unfolding behavior compared to thinner films with excessively rapid diffusion or thicker films with potentially hindered water transport[42]. Consequently, 0.07 mm was chosen as the standard film thickness for subsequent investigations. To assess their suitability for soft robotics, CHT films were intricately patterned and subjected to cyclic folding-unfolding actuation within a 1-2 minute timeframe (**Fig. S3**). This maneuverability highlights the films' remarkable shape-morphing capabilities and potential for integration into soft robotic systems. Importantly, the folding behavior can be precisely programmed by tailoring the AR (length-to-width ratio) of the patterned structures, while the actuation speed can be strategically controlled through the film thickness. This level of tunability positions CHT films as promising candidates for developing advanced soft robots with complex and dynamic functionalities (**movie S7-S11**).

Biocompatibility is crucial for biomedical applications. Our CHT film addresses this concern by eliminating glutaraldehyde, a cytotoxic crosslinking agent commonly used in similar chitosan films reported by Hue et al.[36] and Debta et al.[43] This crosslinking agent, while effective in inducing shape changes upon water absorption, raises concerns regarding cytotoxicity and limits the applicability of these materials in biomedical fields. To assess cytocompatibility, we employed the Alamar Blue assay with NIH-3T3 fibroblasts after 24 and 48 hours of incubation (Fig. 2A). The results demonstrated good cell viability. This finding was further corroborated by 3D cell culture experiments (Fig. 2B). Live/dead staining confirmed high cell viability on the chitosan film surface (Fig. 2C-a). Additionally, nuclei and F-actin staining revealed intact cell morphology, indicating minimal disruption to the fibroblasts cultured on the film (Fig. 2C-b). These results collectively establish the cytocompatibility of our chitosan film, opening doors for its application in biomedical fields such as drug delivery and deployable devices.

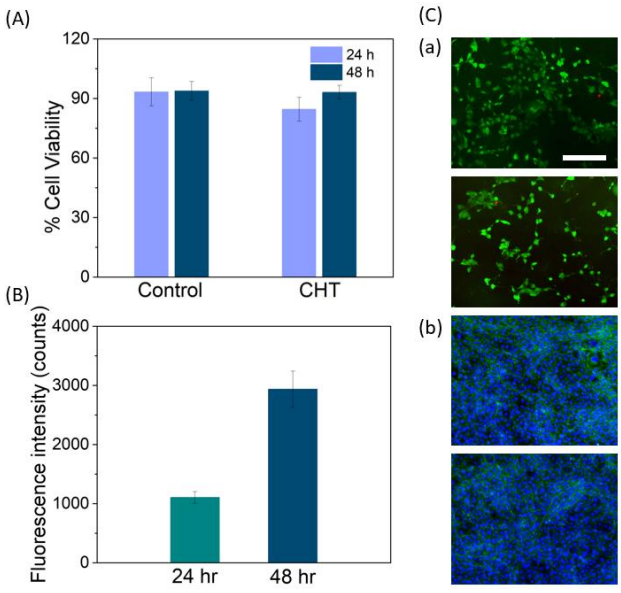

Figure 2
(A) 2D cell culture - % Cell viability of control and CHT film. (B) 3D cell culture graph. (C) (a) Qualitative live (Calcien; green)/dead (PI; red) analysis and (b) cytoskeletal staining of NIH-3T3 cells using F-actin (green)/nuclei (blue) upon treatment with CHT films for 48 h.

CHT films demonstrate directionally dependent high affinity for water absorption. The presence of acetic acid facilitates the protonation of amine groups, transforming them into positively charged ammonium cations ($-NH_3^+$)[44]. These enhance the film's hydrophilicity, promoting water uptake and diffusion. Due to their small size, water molecules readily penetrate the biopolymer film, disrupting weak hydrogen bonds within the network[45]. This enables pore expansion, facilitating further water uptake. However, this process can also contribute to the film's degradation over time. Immersion in water resulted in the uniform expansion of the CHT film, indicating consistent water diffusion throughout the material at all measured time points (**Figs. S4-S6**). The 0.07 mm thick film achieved a remarkable 741% increase in its initial area within 4 minutes. Films of lower thicknesses also exhibited swelling at all time points; however, the most significant increase occurred within the first 80 seconds, with a subsequent decrease in the rate of swelling observed thereafter. Shape deformation of the film upon partial contact with water is attributed to diffusive hydration[38]. This process is relatively slow and can be further impeded by forming pores within the film. The dried CHT film exhibits a high propensity for water diffusion. The unilateral exposure of the film's bottom surface to water triggers a self-folding phenomenon owing to the development of in-plane hydrostatic pressure[46]. This pressure gradient manifests as a differential strain across the film's surface layers, inducing a higher level of stretching at the bottom surface (film-water interface) compared to the top surface (film-air interface), which is ultimately responsible for the film's folding behavior. To elucidate the underlying mechanism of this diffusive absorption process, cross-sectional scanning electron microscopy (SEM) images were obtained **(Fig. 3A).** SEM images were captured at three different time points (**Fig. 3A**; **a**- before water exposure, **b**- during folding, and **c**-after unfolding) in the folding-unfolding dynamics. **Fig. 3A-a** reveals a compact and non-porous region across pristine CHT film, where chitosan units are densely packed following solvent casting and drying. As soon as water diffuses into the film unilaterally, differential strain within the structure will facilitate diffusion, confirmed by the presence of sparsely and densely cross-linked regions (**Fig. 3A-b**). The folding process is completed when water molecules have traveled to the top (**Fig. 3B**). Disruption in the structural gradient commences the unfolding process as the films attempt to revert to their most favorable confirmation **(Fig. 3A-c)**. To further substantiate our hypothesis of the diffusive hydration-induced differential gradient across film, one film was placed onto the surface of the water, and another film was completely immersed (**Fig. S7**). The CHT film floated onto the water surface depicted a similar folding-unfolding dynamic (1° θ~720°), while the θ of immersed films was dramatically low, i.e., <250° (**Fig. S7B & movie S1 & S12**). The intrinsic asymmetry of the film owing to spontaneous drying at ambient conditions could be utilized to develop bilayer films with tailored compositions. An AFM nano-indentation study estimated the elastic modulus for dried CHT film's top (105.722 MPa) and bottom (37.452 MPa) surfaces (**Fig. S8**). We have previously observed and documented this behavior in the solvent-casting method of biopolymers[36]. As developed, CHT films open avenues for advanced water-responsive materials such as surgical reports, gripping, or targeted delivery systems.

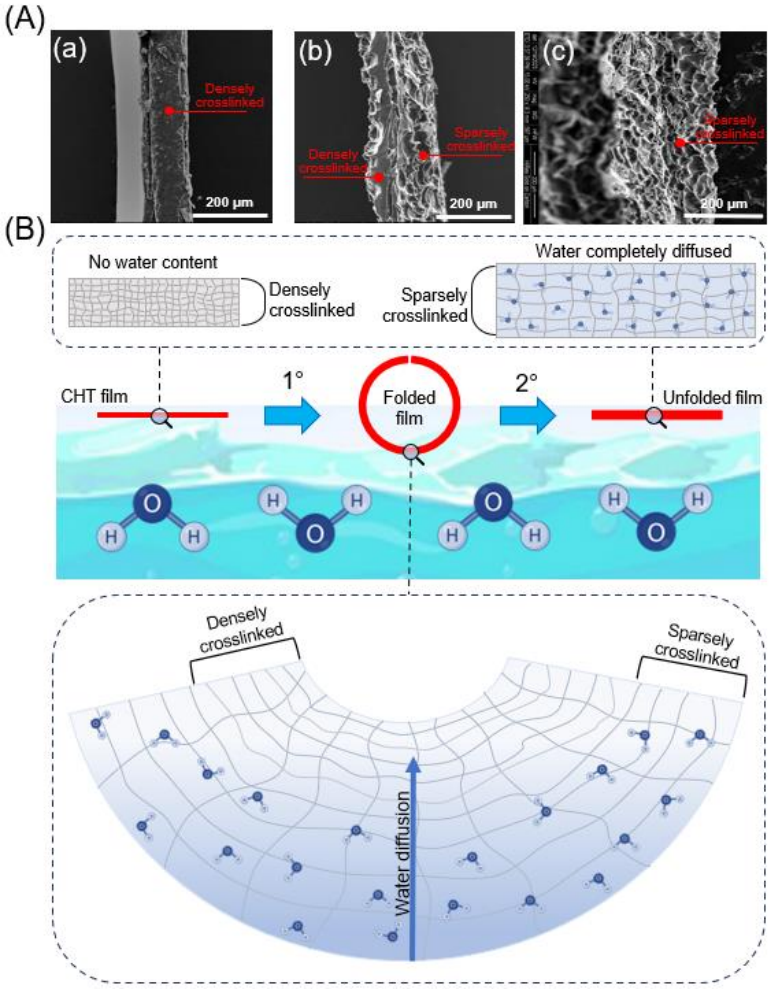

Figure 3

(A) SEM images of the cross-section of CHT film (a) before, (b) during, and (c) after folding. (B) The diffusion mechanism of water into the film causes shape deformation.

Imperfections within the amorphous polymer matrix, arising from the non-ideal packing of polymer chains and the absence of crystalline regions, contribute to the formation of free volume[47]. This accessible volume and its distribution throughout the matrix are crucial in the diffusion process[48]. So, the size of the diffusing solvent molecule immensely influences this process[38]. CHT films exhibit a striking contrast in their response to water and ethanol. The exposure to water induces significant shape deformations within 60 s (**refer to Fig. 1C**). In contrast, the shape and size of the films (AR=1 and AR=60) remain unchanged in ethanol, even after extended periods (>40 min) (**Fig. S9 & movie S13 and S14**). This dehydrating property is employed to "arrest" the water-induced intermediate deformed state of the CHT film upon transfer to ethanol **(Fig. 4A)**. Subsequent immersion into the water allows the unfolding process to resume, yielding the film's native state (**movie S15**). Furthermore, the SEM images revealed the obvious dehydration nature of ethanol, which leads to the closure of all the pores formed by water diffusion, thereby allowing the arrest of the deformed state of CHT film at any given (**Fig. 4B**). Solvent-induced arrest can be attributed to the larger size and weaker solubility of ethanol molecules to chitosan compared to water, limiting their interaction with the CHT film's functional groups. Moreover, the extent of hydrogen bonding of ethanol and water is higher than that of chitosan molecules and water[49].

The response of CHT films, characterized by the presence of -NH_2 and -OH groups, exhibits a strong dependence on the surrounding pH. Therefore, we investigated the effect of pH on the shape-morphing behavior of CHT films. As expected, CHT films underwent a systematic shape-deformation in a neutral pH (~7); however, they revealed an accelerated deformation and degradation in acidic conditions (pH =~3.5) (**Fig. S10**). This phenomenon can be attributed to the enhanced protonation of amine groups (-NH_2) upon exposure to acetic acid. The resulting increase in -NH_3^+ cations renders the film more soluble in the acidic environment, leading to faster degradation[50]. Notably, the rolling (26 s) and unrolling (46 s) process in acidic pH is completed in less than the time observed in neutral conditions while achieving a comparable maximum bending angle (θ_{max}) of approximately 1800° (**movie S16**). Under acidic conditions, the film undergoes accelerated degradation, resulting in a decrease in thickness and a subsequent enhancement of diffusion. Unlike neutral and acidic pH, CHT films exposed to basic environments (pH 11) displayed a distinct response (**Fig. 4C-b**). CHT films did not swell or degrade owing to the deprotonation. However, a bi-directional shape deformation with a θ_{max} significantly lower than that observed in neutral or acidic conditions (θ_{max} = 700°) is observed. This deformation involves the previously observed 1° and 2° folding, along with an additional tertiary deformation (folding in the opposite direction, denoted as 3°). The observed 3° deformation of the CHT film is hypothesized to be driven by a deprotonation process. Exposure to the basic pH solution likely facilitates the diffusion of hydroxide ions, potentially establishing an in-situ gradient responsible for the initial 1° and 2° deformation stages. The 3° deformation itself is attributed to the conversion of protonated amine groups (-NH_3^+) within the chitosan structure back to their neutral (-NH_2) state. This effectively reverses the protonation that occurs in acidic environments and returns the film to a more pristine chitosan-like state. This transformation is accompanied by a reduction in water solubility, suggesting a transition towards a more hydrophobic and structurally rigid conformation. The deprotonation reaction is thus postulated to be the main mechanism governing the unique 3° folding behavior observed in the CHT film. (**movie S17**).

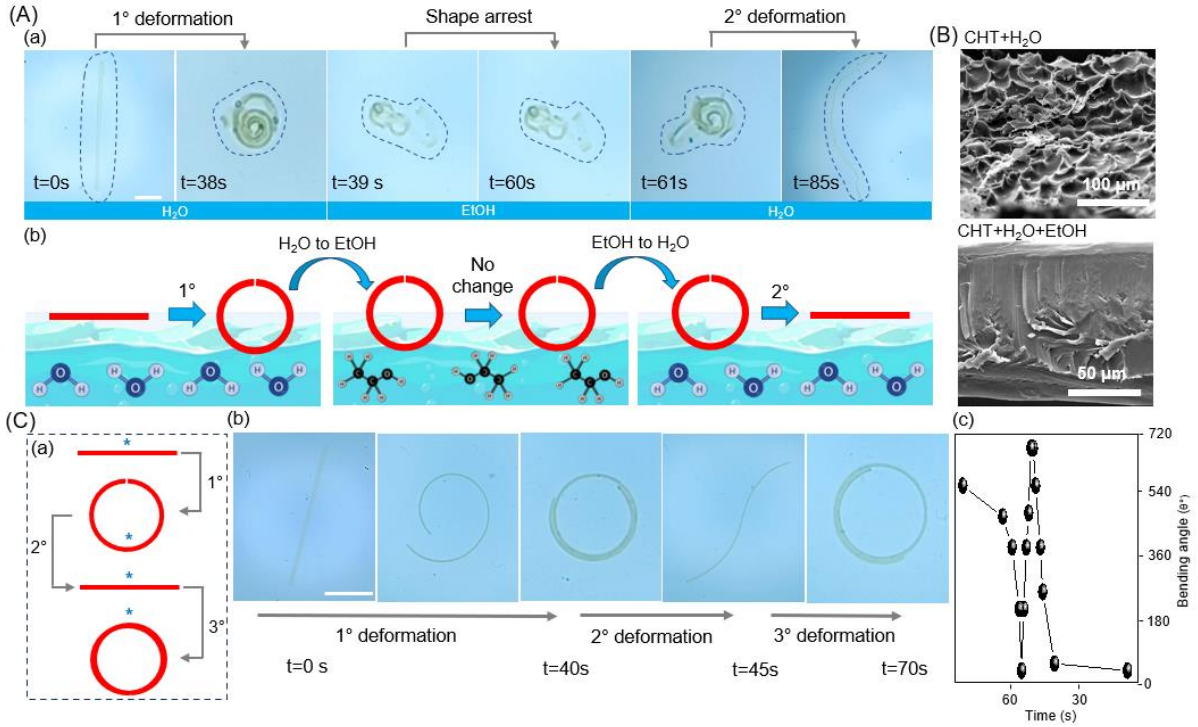

Figure 4

(A) (a) Experimental – (b) Schematic shape arrest method by transferring AR=30 strip into water-ethanol-water. (B) (a) SEM image of hydrated CHT film, (b) Dehydrated CHT film after added to

ethanol. (C) (a) Schematic showing the 1°, 2°, and 3° transformation, (b) Shape-morphing behavior of AR=30 films in pH=11 (c) Corresponding bending angle.

We used the individual frames from the videos (**Movies S1-S4**) capturing shape deformations of the CHT films with different aspect ratios to quantify the changes in out-of-plane bending angles during the corresponding shape deformations. Unlike multiple deformation (1°, 2°, and 3°), the theoretical model adapted for validation in this work is limited to 1° deformation[51]. Therefore, a different methodology for experimental calculation was employed to match the theoretical model. Experimental data with a new methodology for CHT films with 4 different aspect ratios (1, 6, 30, and 60) morphed into tube, helical, spiral, and dual spiral geometries upon unilateral contact with the water surface was obtained (**Fig. 5A**) [X]. The schematic representation shows that the final bending angle for the deformed CHT strips is measured as the total degree of deviation (θ) from the original linear position (the blue dashed line). Using image analysis, the changes in bending angle with time for the different films were measured from the onset of bending (**Fig. 5B**).

We validated the aspect ratio-dependent bending behavior of CHT films by adapting a theoretical framework based on Timoshenko's bilayer beam theory[52]. According to this theory[52], the curvature of a bilayer strip is related to the stiffness ratio and thickness ratio of the two layers using the following relation:-

$$k = \frac{\Delta\alpha}{h}\frac{6(1+m^2)}{3(1+m^2)+(1+mn)(m^2+\frac{1}{mn})} \quad (1)$$

Where k denotes the curvature of the strip, h is the total thickness, Δα the is the mismatch between the swelling equilibrium ratios of the two layers, n is the moduli ratio of the layers, and m is the thickness ratio between the two layers[53,54]. The bending angle was computed from the curvature using a simple relation ($\theta = \frac{lk}{2}$), where l represents the length of the CHT strip. In our work, the entire strip is prepared from CHT with graded crosslinking that results in differences in stiffness and morphology at the top and bottom layers (**Fig. S8 and Fig. S12)**. We estimated Δα from the swelling strains (SW_{strain}) measured as follows:

$$SW_{strain} = \frac{SW_t - SW_i}{SW_i} \quad (2)$$

Where SW_t is the swelling area at time t and SW_i is the initial area of the strip at time t=0. Results showed a nonlinear variation with time and could be estimated using a quadratic fit (**Fig. 5B**). [It is to be noted that– swelling data has been used here for the films of l x b x h = 90 mm x 90 mm x 0.07 mm]. Next, we used an equation to quantify the variation in curvature and corresponding bending angles by performing a parametric sweep for different values of *m* (thickness ratio) to identify which values of m match the experimentally obtained results for CHT strips with different ARs.

Our theoretical investigations show that the experimental results lie close to the parametric curves, specifically for m~10. Finally, to investigate the AR-dependent variation in the CHT strip deformations for all 4 cases (AR = 1, 6, 30, and 60), we slightly modified equation 1 by introducing a function (i.e., aspect ratio dependent *f(AR)*) in the equation and used it to fit the experimental results. For a specific value of m, using a constrained optimization-based approach, *fmincon* in MATLAB (Version 2022B. Natick, MA). The modified form of equation 1 is provided as

$$k = \frac{\Delta\alpha}{h}\frac{6(1+m^2)}{3(1+m^2)+(1+mn)\left(m^2+\frac{1}{mn}\right)}f(AR) \quad (2)$$

Where a nonlinear form of the aspect-ratio dependent function was used, such that

$$f(AR) = AR^b + c$$

Our results indicate that for m=11, exponent b= 0.0167, and the constant term c =0, the best model fits were obtained for all 4 cases using a single equation (**Fig. S13**). The R^2 values were relatively higher for the higher AR values, particularly for the spiral and double spiral shapes. Such results provide useful insights into the mechanics of AR-dependent bending of CHT strips upon exposure to water.

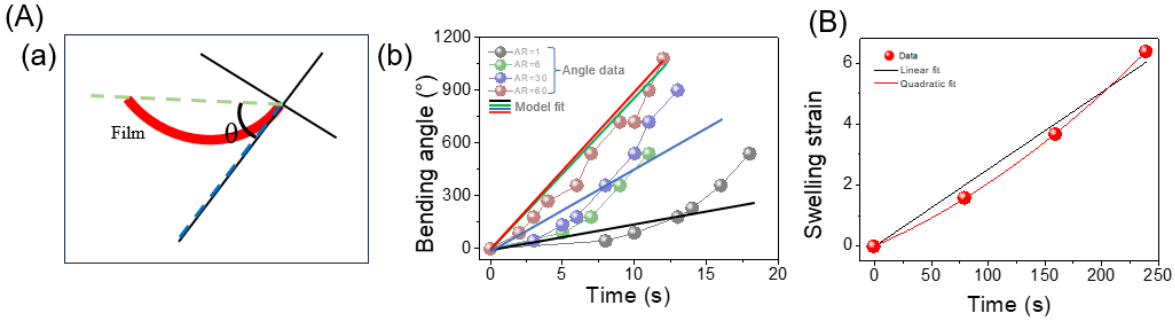

Figure 5
(A) (a) scheme for calculating bending angle, (b) Bending angle calculated and computational model fit. (B) Swelling strain plot with computational linear and quadratic fit.

As developed, CHT-derived soft microrobots exhibit remarkable shape-shifting capabilities that solvent exchange can precisely control. The desired shapes can be achieved and arrested at a given point by leveraging ethanol-induced dehydration-led diffusive hydration. This unique property structural deformation opens doors to a wide range of potential applications across various fields. For instance, the development of a chemo-mechanical sensor for alcohol detection. The sensor probe, i.e., CHT films, utilizes the contrasting response to water and ethanol (**Fig. 6**). We designed a "strip-on-a-drop" model in which a polymer strip (CHT film; AR=12; lxbxh- 24 mm x 2 mm x 0.07 mm) requires only a drop of the sample for semiquantitative detection of alcohol content (**Fig. 6A**). The experimental setup consists of a small hydrophobic substrate that can hold a drop (100-150 µL) of the test sample solution. Then, a CHT film placed on top of the droplet starts to bend due to molecular diffusion from the center of the strip (**Fig. 6A-a**). Change in the bending angles was monitored and digitally captured in the camera until the sum of θ on both sides (θ_1 & θ_2) reached 125° (**Fig. 6A-b**). The extent of bending is affected by the alcohol content in the drop (**Fig. S14)**.

Analysis of the bending angle time series using the custom MATLAB code revealed the influence of ethanol concentration on CHT strip response. The peak angular orientations (θ_1 and θ_2) obtained from the Fourier space analysis quantified the acute and obtuse bending angles, respectively. The sum of θ_1 and θ_2 with no. of frames is plotted (**Fig. 6B-a**). These values, along with their temporal evolution, will elucidate the concentration-dependent bending behavior of the CHT strips in ethanol solutions.

The effect of ethanol concentration (0% to 80%) on the bending behavior of the CHT film was systematically investigated using strips (AR=12) cut out of CHT film. As shown in **Fig. 6B-a**, exposure to pure deionized water (0% EtOH) resulted in a θ_{max} of 125° within 15 seconds. Interestingly, films exposed to ethanol solutions (10/20/35/50/65% vol./vol%) displayed the same θ_{max} but with

progressively delayed response times (18/21/33/65/108 seconds). In 80% of ethanol concentration, the strip does not show any bending. Hence, 65% is taken as the final value, and 80% is not considered for the sensing parameter. The bending angle was calculated from the videos (movies S18-S23), and the R-square value through different plots (percentage of ethanol against $(\theta-\theta_0) / \theta_0$ and time (s)) (**Fig. S15**).

In addition to time, bending angle is another variable that decreases with increasing ethanol concentration at a given contact time (**Fig. 6B-a**). Further, a reported strip-on-a-drop model was utilized to analyze the concentration of alcohol in a commercial alcohol beverage (Whiskey, brand, and model) to test the sensitivity of the designed sensor for unknown samples. As shown in **Fig. 6C-a**, the bending angle of the CHT film for the unknown alcoholic beverage was determined to be 125° within 58 s, corresponding to 41% of alcohol, as per standard calibration curve ($(\theta-\theta_0)/\theta_0$ vs percentage of ethanol; **Fig. 6C**). Obtained result matched with the commercial value (40%; vol./vol%), validating our "strip-on-a-drop" model. Nevertheless, non-selectivity towards alcohol is still a challenge that needs to be addressed. Similar to how the sensor responds to alcohol detection, it can potentially detect other water-based solvents containing ions due to their ability to reduce the diffusion rate. This method offers several advantages, including rapid results and minimal sample requirements, portability, and ease of operation. These potential applications and the identified challenges provide valuable insights for future research directions to optimize CHT film properties and explore their capabilities in various fields (**movies S18-S23**)

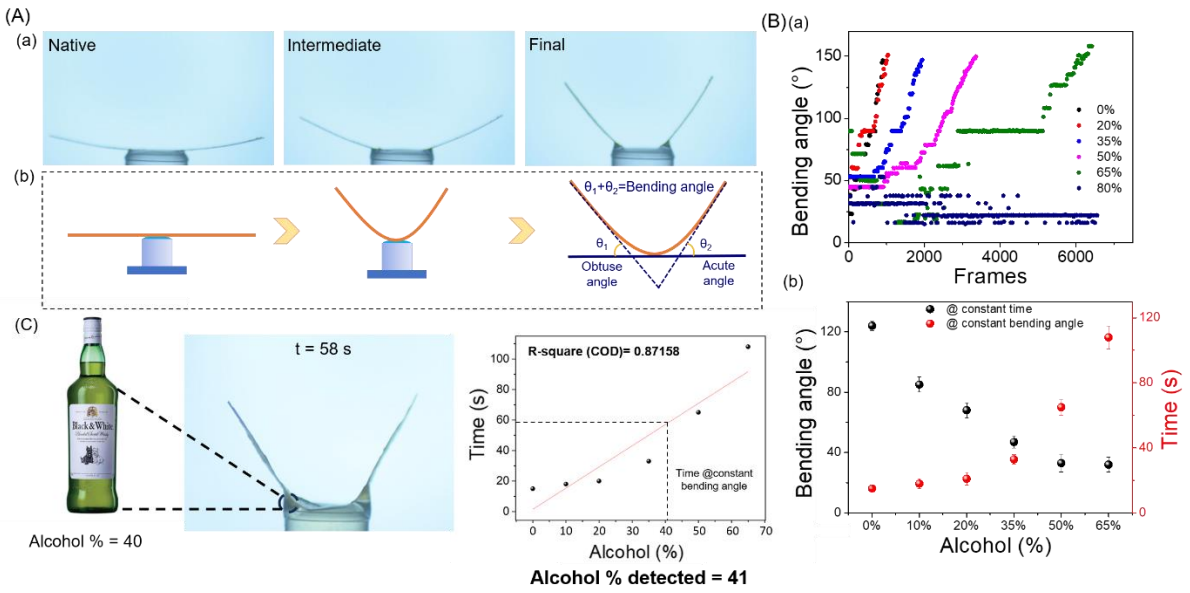

Figure 6

(A) (a) Bending of AR=12 CHT strips on contact with the sample (droplet), (b) Scheme for detecting the bending angle. (B) (a) Calculated bending angles with the frames. (b) Graph showing the change in (a) Time (s) and Bending angle (°) with percentage of alcohol. (C) Alcohol % detection of real-time sample

3 Conclusion

This study presents a significant advancement in biocompatible shape-morphing materials with the development of a novel monocomponent chitosan film. Fabricated through a cost-effective solvent casting technique, this film surpasses the limitations of 3D printing methods commonly employed for such materials. Importantly, eliminating cytotoxic crosslinking agents like glutaraldehyde addresses biocompatibility concerns present in previous work. The chitosan film exhibits exceptional shape-morphing capabilities. It demonstrates rapid and reversible responses to water gradients, facilitated by

a spontaneous diffusion process and this responsiveness can be further tailored by manipulating the film's aspect ratio, enabling programmable control over folding patterns. Additionally, arresting the deformed state via solvent exchange offers a promising avenue for precise locomotion control in potential soft robotic applications. Beyond its shape-morphing capabilities, the film demonstrates potential as a versatile sensing platform. The demonstration of a "strip-on-a-drop" model utilizing digital image processing effectively detected alcohol content. The film's exceptional performance, characterized by rapid shape changes and high bending angles, surpasses previously reported materials. With its programmable shape control, responsive actuation, and sensing capabilities, this novel biocompatible platform paves the way for significant advancements in various fields. Future investigations will explore integrating these films with diverse actuating mechanisms to further enhance their functionality in soft robotics. Further exploration of developing more complex sensing applications has the potential to impact soft robotics, microfluidics, and lab-on-a-chip technologies significantly.

4 Experimental Section

Materials.

Chitosan powder (low molecular weight) and Acetic acid>99%, NaOH pellets were supplied from Sigma-Aldrich. Ethanol (99.9%) is from SN chemicals, and DI water is from in-house. A petri dish of size 90mm was used for pouring the chitosan solution to prepare the film.

Fabrication of CHT film.

Chitosan solution was prepared by mixing 1% (w/v) chitosan in water with 5% (w/v) of acetic acid and stirring at room temperature until a uniform solution was obtained. The prepared solution is poured into the Teflon plates and kept for slow solvent evaporation until it is dried to get CHT film.

Physiological characterization of the film

Scanning Electron Microscopy.

The CHT films have been made in contact with water and freeze-dried at -80°C. Following that, the sample has been lyophilized to remove the water content completely. To see the cross-section, the sample has been dipped into Liq. N_2 to cut it cross-sectionally. Before the SEM analysis, the samples were placed on the metal stub and sputter-coated with gold. The images were recorded in ESEMQUANTA

Indentation study.

The surface morphology of the CHT films was investigated using Atomic Force Microscopy (AFM) (Park Systems NX-10) coupled with an inverted optical microscope and an X–Y flat scanner (100 mm x 100 mm). A spherical SiO_2 probe with a radius of 2500 μm was used for the analysis. The elastic modulus of both film surfaces was determined to understand the stiffness anisotropy arising from the solvent casting process. Measurements were performed at five randomly chosen locations on each sample. The elastic modulus was calculated using the Hertzian model implemented within the XEI software. A CONTSCR cantilever with a known spring constant of 0.2 N/m was employed, and the indentation depth was precisely controlled at -1 μm during analysis. A contact depth of 3 μm was maintained throughout the measurements.

Dynamic Mechanical Analysis.

The static tensile mechanical properties of the gels were evaluated using a dynamic mechanical analyzer (DMA, TA Instruments Q800) operating in controlled force mode. Chitosan hydrogels (CHT films) were secured with a preload of 0.01 N. Subsequently; a uniaxial tensile force was progressively applied at a constant rate of 0.1 N mm^{-1} until specimen rupture. The Young's modulus, representing the material's stiffness, was determined from the initial linear region of the resulting stress-strain curve. Additionally, the strain at failure, indicative of the material's maximum deformation capacity, was extracted from the same plot.

Swelling Studies.

The water absorption capacity of the fabricated chitosan films (CHT) was investigated using a gravimetric approach. Square-shaped samples (9 mm x 9 mm) were obtained by precisely cutting the films. To assess the swelling behavior, the films were submerged in water, and their length and breadth were meticulously recorded at consistent time intervals of 80 seconds. The extent of water uptake was quantified by comparing the calculated area of the film at each time point.

Shape deformation studies.

The impact of film geometry on deformation behavior was evaluated by investigating the shape changes of films with varying aspect ratios (AR). Samples were precisely cut into different geometries, encompassing a range of AR values from 1 to 60. To assess the influence of the solvent, the film deformation behavior upon contact with water and ethanol was examined. Additionally, the effect of solution pH on deformation was explored by immersing the films in solutions with controlled pH values of 3, 7, and 11. The prepared solutions encompass acidic (acetic acid), neutral (water), and basic (NaOH) environments. The resulting shape deformations were captured using a camera for further analysis. The bending angle of all the experiments is calculated and plotted against time.

Cytotoxicity studies.

The potential cytotoxicity of the CHT film was assessed through direct cell contact. Initially, cells were seeded into 48-well plates at a controlled density of 2.5 x 10^4 cells per well. Following a 24-hour culturing, the film was sectioned into 1 cm x 1 cm squares and submerged in the cell culture medium. Control groups were maintained with medium alone for comparison. The cells were then further incubated for 24 hours under standard conditions (37 °C, 5% CO2, humidified incubator). The alamarBlue assay (alamarBlue Cell Viability Reagent, DAL1025) was employed to evaluate cell viability after exposure to the CHT film. Following co-culture, the original cell culture medium and the CHT film were removed and replaced with 200 µL of fresh medium. Subsequently, 20 µL of alamarBlue reagent was added to each well, followed by a 4-hour incubation at 37 °C and 5% CO2. Finally, the absorbance was measured using a microplate reader at a wavelength of 570 nm.

3D cell culture.

NIH 3T3 cells were cultured onto the surface of pre-prepared CHT films measuring 1 cm x 1 cm. Cell adhesion and growth were investigated by allowing the cells to proliferate for designated time periods of 24 and 48 hours. Fluorescence microscopy was employed to visualize and analyze the cellular morphology following staining with DAPI and Actin.

Live-dead analysis.

To assess cell viability, a Live/Dead assay kit (Live/Dead, Invitrogen™, Carlsbad, CA, USA) was employed following the manufacturer's established protocol. This assay utilizes two fluorescent probes: calcein AM (0.5 µL), which specifically stains live cells, and ethidium homodimer-1 (2.0 µL) for identifying dead or dying cells. The dyes were first diluted in 997.5 µL of phosphate-buffered saline (PBS) to create the working solution. Subsequently, this solution was added to the cell samples, followed by a 40-minute incubation period under dark conditions at 37 °C in a humidified incubator with 5% CO2. This incubation allows for the cellular uptake of the respective dyes. Visualization and evaluation of the stained cells were performed using an epifluorescence microscope (ZEISS Axio Scope.A, Carl Zeiss AG, Oberkochen, Germany) equipped with 4x and 10x objective lenses. Image acquisition was facilitated by the ZEN 2012 software (Carl Zeiss AG, Oberkochen, Germany). Finally, the captured images were analyzed using ImageJ software for further quantification or observation.

Cytoskeleton staining.

After 24 and 48 hours of cell culture, samples were removed from the medium and underwent a series of washing and staining steps to visualize cell attachment and distribution on the CHT

films. This involved rinsing with PBS to remove media residue and fixation with paraformaldehyde to preserve cell morphology. Permeabilization with Triton X-100 then facilitated the penetration of staining agents. A dual staining process was employed: DAPI stained cell nuclei, while Alexa Fluor 488 Phalloidin specifically highlighted the F-actin cytoskeleton, allowing visualization of cell spreading on the scaffolds. After the excess stain was removed with PBS, the processed samples were evaluated using an epifluorescence microscope (ZEISS SCOPE system) with 4x and 10x objectives to assess cell dispersion within the control and test group scaffolds (n=3).

Alcohol sensor.

To assess the influence of ethanol concentration on film bending, CHT films with an aspect ratio of 12 were prepared and exposed to a series of ethanol solutions with varying concentrations (0%, 10%, 20%, 35%, 50%, 65%, and 80%). The time-dependent bending behavior of the films upon exposure to each solution was recorded and subsequently plotted for analysis.

Quantification of bending angle for a "strip-on-a-drop" model using MATLAB software

We used videos (refer to **Movies S18-S23**) of CHT strips (AR=12) placed on a droplet (~100 µL) containing varying concentrations of ethanol (0%, 10%, 20%, 35%, 50%, 65%, and 80%) to quantify the time-dependent changes in bending angle of the strips. Firstly, we extracted individual frames (~30 frames per second) from each video individually and quantified the bending angle with time using a custom code written in MATLAB (Version 2022B. Natick, MA), adapted from earlier reported work[55]. The individual frames were typically binarised, and some fundamental image-processing techniques were implemented to minimize the background noise. Following these steps, we used Fast Fourier Transformation to convert the individual frames into Fourier space. Next, the power spectrum was computed, and the corresponding spatial frequencies and angular orientations were obtained in the Fourier space using a wedge-shaped orientation filter[56]. From the overall angular orientation distribution, the peak angular orientation within the 0-90º region was used to quantify the acute bending angle (θ_1), and subsequently, the obtuse angle (θ_2) was also quantified (90-180º) region. The analysis was performed for the entire video length, and at least 3 frames per second were considered for all groups to obtain the dynamics of bending angle over time for the CHT films placed in different concentrations of ethanol.

CrediT authorship contribution statement

Kailas Mahipal Malappuram: Writing – review & editing, Writing – original draft, Visualization, Investigation, conceptualization. **Aritra Chatterjee:** Writing – review & editing. computational and Matlab studies. **Srishti Chakroborty:** Experimentation and cell culture studies. **Souvik Debnath:** Cell culture studies. **Kaushik Chatterjee:** Writing – review & editing, Supervision, Resources, Funding acquisition. **Amit Nain:** Writing – review & editing, Validation, Supervision, Resources, Project administration, Funding acquisition.

Acknowledgments

The authors acknowledge the assistance of Ms. Monisha Vashisht for the AFM studies in the Department of Bioengineering, IISc. This work was supported by the Department of Science and Technology (DST) sponsored Innovation in Science Pursuit for Inspired Research (INSPIRE) Faculty Programme (DST/INSPIRE/04/2021/001535). The authors acknowledge support from the Science and Engineering Research Board (SERB), Government of India (IPA/2020/000025).

Conflicts of Interest

The authors declare no conflict of interest. A patent application has been filed.

Open Research

Data Availability Statement

The data underlying the results presented in this study are available within the main text and/or supplementary materials. Additional data will be made available by authors on request.

References

[1] S. H. Han, S. Lim, K. Ryu, J. Koo, D. Kang, K. Jeong, S. Jeon, D. Kim, *Adv. Funct. Mater.* **2023**, *33*.

[2] S. Bonardd, M. Nandi, J. I. Hernández García, B. Maiti, A. Abramov, D. Díaz Díaz, *Chem. Rev.* **2023**, *123*, 736.

[3] X.-Q. Wang, G. W. Ho, *Mater. Today* **2022**, *53*, 197.

[4] I. P. S. Qamar, K. Stawarz, S. Robinson, A. Goguey, C. Coutrix, A. Roudaut, In *Proceedings of the 2020 ACM Designing Interactive Systems Conference*, ACM, New York, NY, USA, **2020**, pp. 1943–1958.

[5] C. J. Eger, M. Horstmann, S. Poppinga, R. Sachse, R. Thierer, N. Nestle, B. Bruchmann, T. Speck, M. Bischoff, J. Rühe, *Adv. Sci.* **2022**, *9*.

[6] R. Tang, W. Gao, Y. Jia, K. Wang, B. K. Datta, W. Zheng, H. Zhang, Y. Xu, Y. Lin, W. Weng, *Chem. Sci.* **2023**, *14*, 9207.

[7] E. Reyssat, L. Mahadevan, *J. R. Soc. Interface* **2009**, *6*, 951.

[8] P. Nardinocchi, M. Pezzulla, L. Teresi, *Soft Matter* **2015**, *11*, 1492.

[9] Q. Zhao, Y. Wang, H. Cui, X. Du, *J. Mater. Chem. C* **2019**, *7*, 6493.

[10] C. Ning, Z. Zhou, G. Tan, Y. Zhu, C. Mao, *Prog. Polym. Sci.* **2018**, *81*, 144.

[11] H. Cui, Q. Zhao, Y. Wang, X. Du, *Chem. – An Asian J.* **2019**, *14*, 2369.

[12] A. Miriyev, K. Stack, H. Lipson, *Nat. Commun.* **2017**, *8*, 596.

[13] C. L. Randall, E. Gultepe, D. H. Gracias, *Trends Biotechnol.* **2012**, *30*, 138.

[14] Q. Zhao, J. Wang, H. Cui, H. Chen, Y. Wang, X. Du, *Adv. Funct. Mater.* **2018**, *28*.

[15] Q. Zhao, J. Wang, Y. Wang, H. Cui, X. Du, *Natl. Sci. Rev.* **2020**, *7*, 629.

[16] K. E. Peyer, L. Zhang, B. J. Nelson, *Nanoscale* **2013**, *5*, 1259.

[17] Y. Wang, H. Cui, Q. Zhao, X. Du, *Matter* **2019**, *1*, 626.

[18] H. Cui, Q. Zhao, L. Zhang, X. Du, *Adv. Intell. Syst.* **2020**, *2*.

[19] S. Wei, T. K. Ghosh, *Adv. Mater. Technol.* **2022**, *7*.

[20] L. Ren, B. Li, G. Wei, K. Wang, Z. Song, Y. Wei, L. Ren, Qingping Liu, *iScience* **2021**, *24*, 103075.

[21] A. Chatterjee, N. R. Chahare, P. Kondaiah, N. Gundiah, *Soft Robot.* **2021**, *8*, 640.

[22] Z. Wang, Y. Chen, Y. Ma, J. Wang, *Biomimetics* **2024**, *9*, 128.

[23] Z. Tian, J. Xue, X. Xiao, C. Du, Z. Han, Y. Liu, *Sensors Actuators B Chem.* **2024**, *410*, 135678.

[24] F. Ahmed, M. Waqas, B. Jawed, A. M. Soomro, S. Kumar, A. Hina, U. Khan, K. H. Kim, K. H. Choi, *Smart Mater. Struct.* **2022**, *31*, 073002.

[25] S. Kim, C. Laschi, B. Trimmer, *Trends Biotechnol.* **2013**, *31*, 287.

[26] H. Cui, N. Pan, W. Fan, C. Liu, Y. Li, Y. Xia, K. Sui, *Adv. Funct. Mater.* **2019**, *29*.

[27] Y. Cheng, K. Ren, D. Yang, J. Wei, *Sensors Actuators B Chem.* **2018**, *255*, 3117.

[28] A. Ding, O. Jeon, R. Tang, Y. Bin Lee, S. J. Lee, E. Alsberg, *Adv. Sci.* **2021**, *8*, 1.

[29] P. Mondal, A. Mandal, K. Chatterjee, *Adv. Mater. Technol.* **2023**, *8*, 1.

[30] S. Naficy, R. Gately, R. Gorkin, H. Xin, G. M. Spinks, *Macromol. Mater. Eng.* **2017**, *302*, 1600212.

[31] M. Champeau, D. A. Heinze, T. N. Viana, E. R. de Souza, A. C. Chinellato, S. Titotto, *Adv.*

Funct. Mater. **2020**, *30*.
[32] A. J. R. Barcena, K. Dhal, P. Patel, P. Ravi, S. Kundu, K. Tappa, *Gels* **2023**, *10*, 8.
[33] A. Joshi, S. Choudhury, V. S. Baghel, S. Ghosh, S. Gupta, D. Lahiri, G. K. Ananthasuresh, K. Chatterjee, *Adv. Healthc. Mater.* **2023**, *12*.
[34] A. Nain, A. Joshi, S. Debnath, S. Choudhury, J. Thomas, J. Satija, **2024**, 1.
[35] A. Nain, S. Chakraborty, N. Jain, S. Choudhury, S. Chattopadhyay, K. Chatterjee, S. Debnath, *Biomater. Sci.* **2024**.
[36] H. Hu, C. Huang, M. Galluzzi, Q. Ye, R. Xiao, X. Yu, X. Du, *Research* **2021**, *2021*.
[37] A. Rath, S. Mathesan, P. Ghosh, *Soft Matter* **2016**, *12*, 9210.
[38] S. Mathesan, A. Rath, P. Ghosh, *J. Phys. Chem. B* **2017**, *121*, 4273.
[39] N. Caruso, A. Cvetković, A. Lucantonio, G. Noselli, A. DeSimone, **2018**.
[40] G. Stoychev, S. Zakharchenko, S. Turcaud, J. W. C. Dunlop, L. Ionov, *ACS Nano* **2012**, *6*, 3925.
[41] S. Alben, B. Balakrisnan, E. Smela, *Nano Lett.* **2011**, *11*, 2280.
[42] C. Zhuang, Y. Zhong, Y. Zhao, *Food Control* **2019**, *97*, 25.
[43] S. Debta, P. Y. Kumbhar, P. Ghosh, R. K. Annabattula, *ACS Appl. Eng. Mater.* **2024**.
[44] D. B. Rorabacher, W. J. MacKellar, F. R. Shu, S. M. Bonavita, *Anal. Chem.* **1971**, *43*, 561.
[45] J. Campbell, A. S. Vikulina, *Polymers (Basel).* **2020**, *12*, 1949.
[46] R. Kempaiah, Z. Nie, *J. Mater. Chem. B* **2014**, *2*, 2357.
[47] M. Usman, A. Ahmed, B. Yu, Q. Peng, Y. Shen, H. Cong, *Eur. Polym. J.* **2019**, *120*, 109262.
[48] D. Hofmann, M. Entrialgo-Castano, A. Lerbret, M. Heuchel, Y. Yampolskii, *Macromolecules* **2003**, *36*, 8528.
[49] Y.-Z. Zheng, Y. Zhou, Q. Liang, D.-F. Chen, R. Guo, *J. Mol. Model.* **2016**, *22*, 95.
[50] C. Nunes, É. Maricato, Â. Cunha, A. Nunes, J. A. L. da Silva, M. A. Coimbra, *Carbohydr. Polym.* **2013**, *91*, 236.
[51] Q. Bian, L. Fu, H. Li, *Nat. Commun.* **2022**, *13*, 137.
[52] S. Timoshenko, *J. Opt. Soc. Am.* **1925**, *11*, 233.
[53] A. I. Egunov, J. G. Korvink, V. A. Luchnikov, *Soft Matter* **2016**, *12*, 45.
[54] A. Lucantonio, P. Nardinocchi, M. Pezzulla, *Proc. R. Soc. A Math. Phys. Eng. Sci.* **2014**, *470*, 20140467.
[55] A. Chatterjee, P. Kondaiah, N. Gundiah, *Biomech. Model. Mechanobiol.* **2022**, *21*, 553.
[56] A. H. Kulkarni, A. Chatterjee, P. Kondaiah, N. Gundiah, *Phys. Biol.* **2018**, *15*, 065005.

Click here to access/download
Supporting Information
MovieS1.mp4

Click here to access/download
Supporting Information
MovieS9.mp4

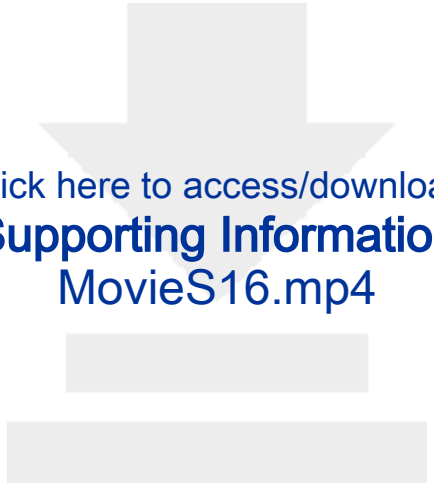

Click here to access/download
Supporting Information
MovieS16.mp4